Mon. Not. R. Astron. Soc. **000**, 1–?? (2014) Printed 11 February 2015 (MN LATEX style file v2.2)

The frequency and infrared brightness of circumstellar discs at white dwarfs

M. Rocchetto[1⋆], J. Farihi[1]†, B. T. Gänsicke[2], C. Bergfors[1]
[1]*Department of Physics & Astronomy, University College London, Gower Street, London, WC1E 6BT, UK*
[1]*Department of Physics, University of Warwick, Coventry CV4 7AL, UK*

arXiv:1410.6527v2 [astro-ph.EP] 10 Feb 2015

Accepted 2015 February 10. Received 2015 January 15; in original form 2014 October 21

ABSTRACT
White dwarfs whose atmospheres are polluted by terrestrial-like planetary debris have become a powerful and unique tool to study evolved planetary systems. This paper presents results for an unbiased *Spitzer* IRAC search for circumstellar dust orbiting a homogeneous and well-defined sample of 134 single white dwarfs. The stars were selected without regard to atmospheric metal content but were chosen to have 1) hydrogen rich atmospheres, 2) $17\,000\,\mathrm{K} < T_{\rm eff} < 25\,000\,\mathrm{K}$ and correspondingly young post main-sequence ages of 15–270 Myr, and 3) sufficient far-ultraviolet brightness for a corresponding *Hubble Space Telescope* COS Snapshot. Five white dwarfs were found to host an infrared bright dust disc, three previously known, and two reported here for the first time, yielding a nominal $3.7^{+2.4}_{-1.0}$% of white dwarfs in this post-main sequence age range with detectable circumstellar dust. Remarkably, the complementary *Hubble* observations indicate that a fraction of 27% show metals in their photosphere that can only be explained with ongoing accretion from circumstellar material, indicating that nearly 90% of discs escape detection in the infrared, likely due to small emitting surface area. This paper also presents the distribution of disc fractional luminosity as a function of cooling age for all known dusty white dwarfs, suggesting possible disc evolution scenarios and indicating an undetected population of circumstellar discs.

Key words: circumstellar matter – stars: abundances – planetary systems – white dwarfs

1 INTRODUCTION

The field of exoplanetary research is one of the most rapidly expanding subjects in astrophysics. The large number of new discoveries made in the past 20 years have led to swift progress and a preliminary characterisation of the Galactic planet population. Current detection techniques enable estimates of exoplanet radius and mass, using mainly the transit and radial velocity methods, but density alone does not yield a unique solution for the bulk composition of the planet (Adams, Seager, & Elkins-Tanton 2008; Valencia, Sasselov, & O'Connell 2007). Transit spectroscopy can also provide some insights into the composition of exoplanet atmospheres (Grillmair et al. 2007; Tinetti et al. 2007) but to date has proved difficult.

In this context, white dwarfs offer a unique laboratory to study exoplanetary compositions. It is now clear that planetary systems around Sun-like and intermediate-mass stars survive, at least in part, the post-main sequence phases of their hosts (Zuckerman et al. 2010). Compelling evidence comes from metal polluted white dwarfs that commonly exhibit closely orbiting circumstellar dust (and sometimes gas) discs originating from the disruption of large asteroids or planetesimals (Farihi, Zuckerman, & Becklin 2008b; von Hippel et al. 2007; Gänsicke et al. 2006; Becklin et al. 2005; Zuckerman & Becklin 1987).

Owing to high surface gravity and negligible radiative forces, heavy elements sink on relatively short timescales within the atmospheres of relatively cool ($T_{\rm eff} \lesssim 25\,000\,\mathrm{K}$) white dwarfs if compared to the evolution timescales (Paquette et al. 1986; Fontaine & Michaud 1979). Hence, the presence of metals in the atmospheres of cool degenerates must be a sign of recent external accretion (Zuckerman et al. 2003). The source of this accreting material was initially attributed to the interstellar medium (Dupuis et al. 1993a; Dupuis, Fontaine, & Wesemael 1993b; Dupuis et al. 1992) or comets (Alcock, Fristrom, & Siegelman 1986), but both theories had trouble in explaining the high and ongoing accretion rates found at hydrogen dominated white dwarfs (Zuckerman et al. 2003). Today accretion from circumstellar material, resulting from the disruption of large asteroids or

⋆ E-mail: m.rocchetto@ucl.ac.uk
† STFC Ernest Rutherford Fellow

© 2014 RAS

minor planets, is, by far, the most compelling explanation for atmospheric metals seen at a large fraction of cool white dwarfs (Veras et al. 2013; Jura 2003).

Metal enriched white dwarfs have become a powerful tool to indirectly analyse the composition of exoterrestrial planetary matter, as their photospheres in principle mirror the composition of the accreted material. As an example of this technique, it was demonstrated that the relative abundances of 15 heavy elements in the atmosphere of GD 362 reflect the composition of a large asteroid that was similar in composition to the bulk Earth-Moon system (Zuckerman et al. 2007). Notably, ultraviolet and optical spectroscopy have shown that metal-contaminated degenerates are, in general, refractory-rich and volatile-poor (Gänsicke et al. 2012; Klein et al. 2010; Desharnais et al. 2008; Dufour et al. 2007; Wolff, Koester, & Liebert 2002), while infrared spectroscopy reveals that the circumstellar dust itself is silicate-rich and carbon-poor (Jura, Farihi, & Zuckerman 2009; Reach et al. 2009; Reach et al. 2005), and thus similar to materials found in the inner Solar System (Lodders 2003). Furthermore, a circumstellar disc that resulted from the destruction of a rocky and water-rich extrasolar minor planet was identified around the white dwarf GD 61 (Farihi, Gänsicke, & Koester 2013), demonstrating the existence of water in terrestrial zone planetesimals that could play an important role in delivering water to the surface of planets.

Detailed modelling of the infrared excesses found at a fraction of metal polluted white dwarfs suggests that the circumstellar dust is arranged in the form of an optically thick but geometrically thin disc, with similar properties to the rings of Saturn (Rafikov & De Colle 2006; Jura 2003). These rings of warm dust are situated within the Roche limit of their host star, as also confirmed by the emission and absorption profiles of gaseous debris discovered at several dusty white dwarfs (Brinkworth et al. 2012; Debes et al. 2012a; Brinkworth et al. 2009; Gänsicke et al. 2006). There is substantial theoretical support for disc creation via tidal disruption of post-main sequence planetary systems, perturbed by unseen planets (Veras et al. 2014, 2013; Debes & Sigurdsson 2002). The transition from disruption to disc is still poorly understood but there are good models for the evolution of these metal dominated discs (Frewen & Hansen 2014; Debes, Walsh, & Stark 2012b; Metzger, Rafikov, & Bochkarev 2012; Bonsor, Mustill, & Wyatt 2011).

After nearly a decade of dust disc discoveries at metal enriched degenerates, the statistical frequency of the phenomenon still suffers from significant observational biases. While the fraction of metal polluted white dwarfs that are currently accreting has been constrained by several unbiased surveys to about 20–30% (Koester, Gänsicke, & Farihi 2014; Zuckerman et al. 2010; Zuckerman et al. 2003), surveys aiming to detect infrared bright dust discs at white dwarfs suffer from considerable biases. The first searches for infrared excesses targeted relatively cool ($T_{\rm eff} \lesssim 25\,000$ K) stars known to be metal-polluted (Farihi et al. 2010; Jura, Farihi, & Zuckerman 2007; Debes, Sigurdsson, & Hansen 2007), and this approach does not permit robust statistics of disc frequency over the entire white dwarf population. With little restriction of stellar effective temperature, wide field surveys such as SDSS, UKIDSS, and *WISE* have found disc frequencies between 0.4 and 1.9% (Girven et al. 2011; Steele et al. 2011; Debes et al. 2011b). On the other hand, more sensitive *Spitzer* observations of K-band bright white dwarfs, without regard to stellar temperature, resulted in a nominal disc frequency of 1.6% (Mullally et al. 2007). A higher frequency of 4.5% was obtained by Barber et al. (2012), by targeting stars in a restricted temperature range where dust detections were expected based on prior surveys. Moreover, the observed sample was fragmented over several instruments and hence the result is difficult to compare with other surveys.

In order to determine definite statistics of the frequency of infrared bright discs at white dwarfs, this paper presents *Spitzer* observations of a well defined sample of 134 young DA white dwarfs in the temperature range $17\,000\,{\rm K} < T_{\rm eff} < 25\,000\,{\rm K}$. Metal abundances for 85 of the stars were also determined in a complementary *Hubble Space Telescope* COS Snapshot program (Koester et al. 2014), and permit the first unbiased statistics of the frequency of circumstellar discs at young white dwarfs.

Section 2 describes the sample selection criteria and *Spitzer* photometry, Section 3 discusses how the spectral energy distributions of the sample stars were obtained and describes those with detected discs. Sections 4 and 5 present the derived disc frequency in the context of complementary *HST* ultraviolet observations and previous surveys, and Section 6 discusses the distribution of the fractional disc luminosity for all known dusty white dwarfs. Section 7 presents notes on the individual objects, and Section 8 gives a short conclusion.

2 OBSERVATIONS

2.1 Sample selection

The sample of hydrogen dominated white dwarfs was selected from the catalogues compiled by Liebert, Bergeron, & Holberg (2005) and Koester et al. (2009), who performed model atmosphere analyses based on optical spectroscopy, providing effective temperature, surface gravity, mass and cooling age. The only criteria for selection were 1) $17\,000\,{\rm K} < T_{\rm eff} < 25\,000\,{\rm K}$ and corresponding young cooling ages of 15–270 Myr, 2) predicted fluxes $F_\lambda(1300\,{\rm \AA}) > 5\times10^{-14}\,{\rm erg\,cm^{-2}\,s^{-1}\AA^{-1}}$ for the corresponding *HST* COS Snapshot survey. As such, the selection was performed only for temperature and brightness, resulting in an unbiased sample of 134 DA young single white dwarfs. The distributions of the fundamental stellar parameters are shown in Figure 1.

2.2 Spitzer observations

A total of 100 sample stars were observed between 2012 May and October in the 3.6 and 4.5 μm bandpasses using the Infrared Array Camera (IRAC; Fazio et al. 2004) onboard the *Spitzer Space Telescope* (Werner et al. 2004) as part of Program 80149[1]. An exposure time of 30 s was used

[1] Five stars were also observed as part of the same Program but are not included in this study. The white dwarf 1929+012 was observed as an ancillary target (see Section 7.2) while four white dwarfs (0933+025, 1049+103, 1335+369, 1433+538) initially considered to be single stars and included in the original sample were

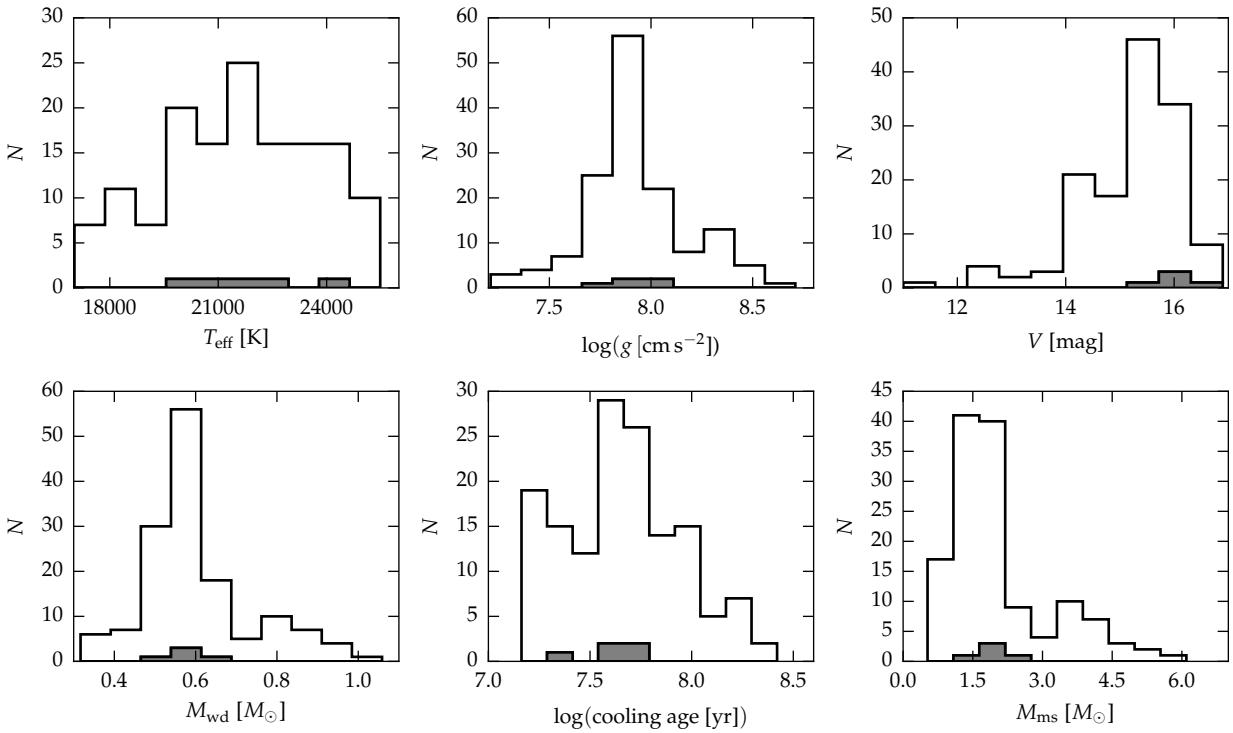

Figure 1. Fundamental properties of the 134 DA stars observed in the *Spitzer* survey. Effective temperature $T_{\rm eff}$ and surface gravity $\log g$ are taken from Liebert et al. (2005) or Koester et al. (2009), and V-band magnitudes are taken from the AAVSO Photometric All-Sky Survey (APASS). Final white dwarf mass $M_{\rm wd}$ and cooling age are derived using evolutionary cooling sequences (Fontaine, Brassard, & Bergeron 2001); the initial main-sequence progenitor mass $M_{\rm ms}$ is derived from $M_{\rm wd}$ and the initial-to-final mass relation (Kalirai et al. 2008). The entire sample of white dwarfs is shown with the unfilled histograms, while the degenerates with infrared detected discs are shown in grey.

for each individual frame, with 20 medium-size dithers in the cycling pattern, resulting in 600 s total exposure time in each warm IRAC channel. The remaining 34 sample stars were previously observed during either the cold or warm mission, and their archival data were analysed.

The analysis of all targets was performed using the 0.″6 pixel^{-1} mosaics (Post-Basic Calibrated Data) processed by the IRAC calibration pipeline version S 18.25.0 which produces a single, fully processed and calibrated image. Aperture photometry was performed using the point source extraction package APEX within MOPEX (Makovoz et al. 2006) and an aperture radius of 4 pixels with a 24–40 pixels sky annulus. Fluxes were corrected for aperture size, but not for colour. For blended sources, point response function (PRF) fitting was performed on the Basic Calibrated Data frames, using the package APEX MULTIFRAME within MOPEX. Fluxes obtained with PRF fitting were compared with the DAOPHOT PSF fitting routine within IRAF for a representative sample, and led to consistent results to within 4%, and always within the relative uncertainties. The measured flux uncertainty was computed by APEX and include the source photon noise and the variance in sky background. A 5% calibration uncertainty is conservatively added in quadrature to all IRAC fluxes. The flux determinations and uncertainties for the science targets, together with the physical parameters of the stars, are reported in the Appendix.

found to host unresolved M dwarf companions and were therefore excluded. Infrared fluxes for these four binaries are reported in the Appendix.

2.3 Additional near-infrared observations

Independent $JHK_{\rm s}$ photometry was also obtained for five targets (Table 1). The stars were observed in 2011 October with LIRIS (Manchado et al. 1998) at the William Herschel Telescope (WHT) and in 2011 August with SOFI (Moorwood et al. 1998) at the New Technology Telescope (NTT), with exposure times of 30, 15, and 10 s at J, H, and K_s respectively. Sufficient dithers were performed for a total exposure time of 270 s at each bandpass for each target. Three standard star fields from the ARNICA catalogue (Hunt et al. 1998) were observed each night for flux calibration. The data were reduced using standard aperture photometry with the IRAF task APPHOT. The flux calibration for all nights was good to 5% or better.

3 DATA ANALYSIS

The spectral energy distributions (SEDs) of the sample stars were constructed with additional short wavelength photometry from a variety of catalogues, including Sloan Digital Sky Survey (SDSS; Ahn et al. 2012), AAVSO Photometric All-Sky Survey (APASS; Henden et al. 2009), Two Micron All

Table 1. Independent JHK_s photometry. All errors are 5%.

WD	J (mag)	H (mag)	K_s (mag)	Instrument /Telescope
1013+256	16.90	17.03	17.15	LIRIS/WHT
0843+516	16.56	16.58	16.49	LIRIS/WHT
0431+126	14.79	14.83	14.94	LIRIS/WHT
0421+162	14.81	14.83	14.89	LIRIS/WHT
1953–175	15.59	15.68	15.73	SOFI/NTT

Sky Survey (2MASS; Skrutskie et al. 2006), UKIRT Infrared Deep Sky Survey (UKIDSS; Lawrence et al. 2007), and Deep Near Infrared Survey of the Southern Sky (DENIS; Epchtein et al. 1999). Additional near-infrared fluxes for a few targets were also obtained from the literature (Barber et al. 2012; Farihi 2009).

The available optical and near-infrared fluxes were fitted with pure hydrogen white dwarf atmosphere models (Koester 2010), kindly provided by the author. The fit was computed by matching the optical and near-infrared best-quality photometric data points with a model spectrum with $\log g = 8$ and effective temperature obtained from Liebert et al. (2005) or Koester et al. (2009), approximated to the closest available model. The Levenberg-Marquardt minimisation algorithm was used to find the best scaling factor.

3.1 Stars with infrared excesses

Amongst the 134 sample stars, a total of five white dwarfs show a significant ($> 4\sigma$) excess in the IRAC bands: 0843+516, 1015+161, 1457–086, 1018+410, and 2328+107. The first three stars have known infrared excesses (Xu & Jura 2012; Farihi et al. 2009; Jura et al. 2007) and are also known to be metal polluted (Gänsicke et al. 2012; Koester et al. 2005), while the infrared excesses at 1018+410 and 2328+107 are reported here for the first time. The presence of a significant excess at the ancillary target 1929+012 (Melis et al. 2011; Debes et al. 2011b; Vennes et al. 2010) is also confirmed. This target, which is not part of the statistical sample, is discussed separately in Section 7, together with notes on individual excesses. The infrared excesses were individually modelled as thermal continua using an optically thick, geometrically thin disc (Jura 2003). Stellar, substellar or planetary companions, and background contamination were confidently ruled out as the excess emission is either too strong (Farihi et al. 2009, 2008a) or the infrared colours are not compatible. The white dwarf radius was estimated from evolutionary models (Fontaine et al. 2001) while the distance was derived using synthetic absolute photometry (Holberg & Bergeron 2006) compared with available optical and near-infrared magnitudes. Fluxes at 7.9 μm were excluded from the fits as these are often contaminated by a strong, 10 μm silicate emission feature, as seen in e.g. GD 362 (Jura et al. 2009) and G29-38 (Reach et al. 2005).

The free parameters in the disc model are the inner disc temperature $T_{\rm in}$, the outer disc temperature $T_{\rm out}$, and the disc inclination i. The radius of the disc at these temperatures can be easily estimated and is proportional to $T^{-3/4}$ (Chiang & Goldreich 1997). In the absence of longer wavelength photometry extending to 24 μm, these three free parameters cannot be well constrained (Jura et al. 2007). A modest degree of degeneracy is found between the inclination and the radial extent of the disc, especially for subtle excesses (Bergfors et al. 2014; Girven et al. 2012). While the inner disc temperature and radius can be well constrained by the 3.6 μm emission, a large set of outer radii and disc inclinations can equally fit the longer-wavelength excess (see e.g. Jura et al. 2007). Two sets of representative models are therefore presented for each star with infrared excess, one corresponding to a relatively wide disc at high inclination and one to a more narrow ring at low inclination. An algorithm for bound constrained minimisation (Byrd et al. 1995) was used to estimate the best fit parameters in both cases.

Table 2. White dwarfs with circumstellar discs in this *Spitzer* survey.

WD	R/d (10^{-12})	$T_{\rm in}$ (K)	$T_{\rm out}$ (K)	$r_{\rm in}$ (R_*)	$r_{\rm out}$ (R_*)	i (deg)
Model 1: High inclinations						
0843+516	3.2	1750	800	14	30	87
1015+161	4.2	1450	900	14	22	85
1018+410	2.9	1600	700	14	32	87
1457–086	2.8	2000	600	10	34	89
2328+107	4.4	1480	1300	14	16	88
Model 2: Narrow rings						
0843+516	3.2	1000	960	24	25	30
1015+161	4.2	1120	1000	18	20	70
1018+410	2.9	1000	940	22	24	40
1457–086	2.8	1000	940	20	21	75
2328+107	4.4	1300	1270	16	17	75

Figure 2 shows the modelled and photometric SEDs of the dusty white dwarfs, and Table 2 gives the fitted disc parameters for the two sets of models. It can be seen that the outer radii of the model discs are all located within the Roche limit of the star ($\approx 1.2\,R_\odot$) where planetesimals larger than $\approx$ 1 km would be tidally destroyed. Moreover, the acceptable values for the inner disc temperatures are in agreement with the temperature at which solid dust grains rapidly sublimate in a metal-rich and hydrogen-poor disc (Rafikov 2012). It is interesting to notice that all models with larger radial extent require improbably high inclinations, all greater or equal to 85° (Table 2). Because it is highly unlikely for all the inclinations to be so confined, most if not all these discs must actually be relatively narrow. Section 6 discusses this evidence in greater detail.

4 THE FREQUENCY OF CIRCUMSTELLAR DEBRIS

The detection of dust at five of 134 sample stars translates to a nominal excess frequency of $3.7^{+2.4}_{-1.0}$% for post-main sequence ages of 15–270 Myr. The upper and lower bounds are calculated using the binomial probability distribution and 1σ confidence level. This frequency is a firm lower limit on the fraction of 2–3 $M_\odot$ stars (the typical progenitors of the white dwarfs in our sample) that form planetary systems. However, complementary *HST* COS observations

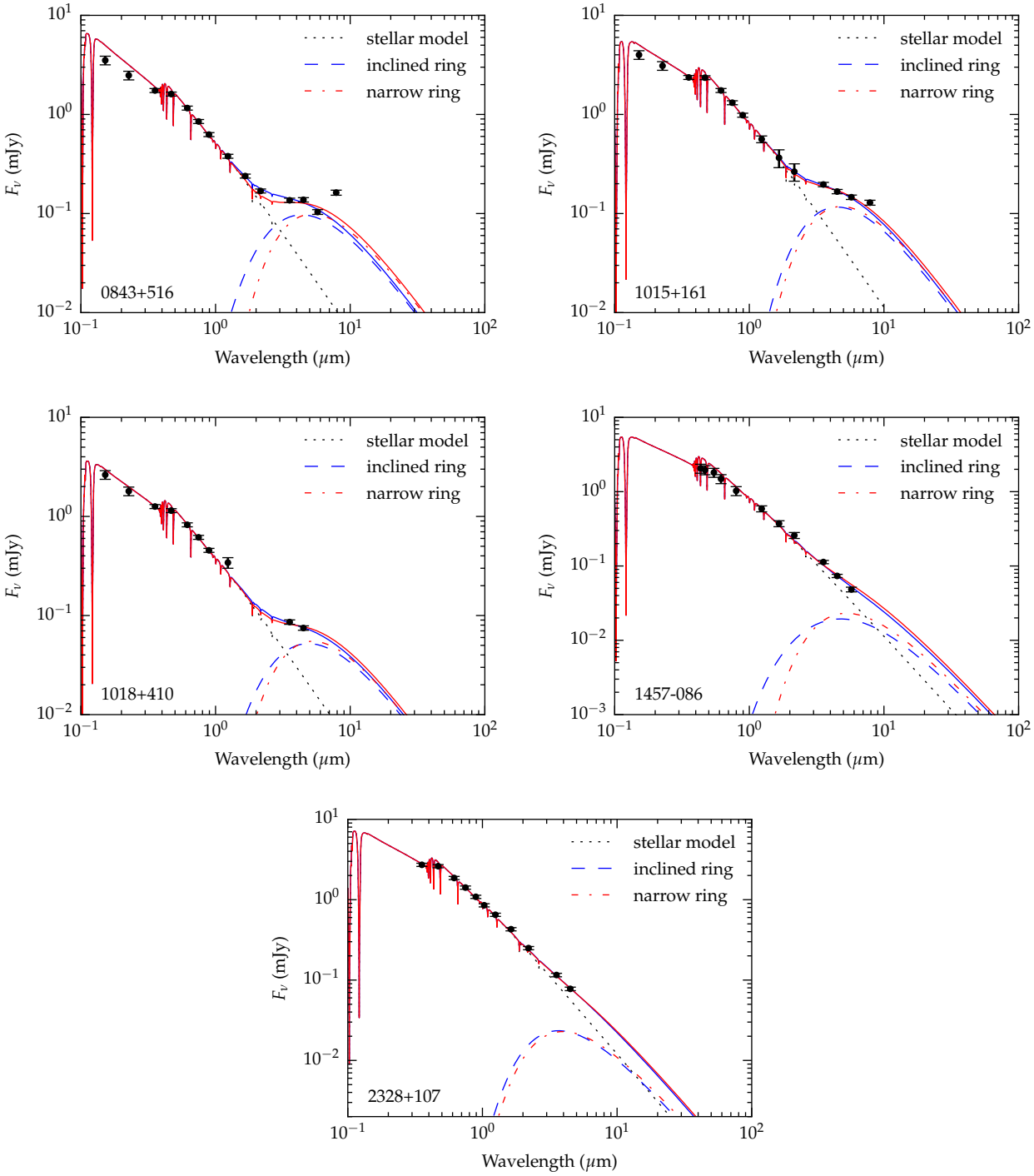

Figure 2. Infrared excesses fit by circumstellar disc models, with parameters listed in Table 2. Stellar atmosphere models are plotted as dot-dashed lines. Dashed lines represent emission from optically thick disc models, and solid lines represent the sum of the stellar and disc model fluxes. Two disc models are plotted for each star, one corresponding to highly inclined discs (blue), one to narrow rings (red). Circle symbols with error bars represent optical and infrared photometry, including IRAC fluxes.

demonstrate that at least 27% of white dwarfs with diffusion timescales of only a few weeks have photospheric metals that require ongoing accretion of a circumstellar reservoir. These findings clearly indicate that the actual fraction of debris discs at white dwarfs is almost an order of magnitude higher, with nearly 90% of discs emitting insufficient flux to be detected by the current infrared facilities, such as *Spitzer*.

4.1 Complementary *HST* COS observations

The entire sample of 134 stars observed with *Spitzer* was also approved as an *HST* COS Snapshot program. Snapshot targets are observed during gaps between regular guest observer programs, and a total of 85 of the 134 white dwarfs were observed between 2010 September and 2013 February within programs 12169 and 12474. The results of the *HST* survey itself are published elsewhere (Koester et al. 2014), and these are summarised briefly here. It was found that amongst these 85 stars, 56% display atmospheric metals: 48 exhibit photospheric Si, 18 also show C, and 7 show further metals. The analysis indicated that for 25 stars the metal abundances may be explained by radiative levitation alone, although accretion has likely occurred recently, leaving 23 white dwarfs (27%) that exhibit traces of heavy elements that can only be explained with ongoing accretion of circumstellar material, in agreement with previous estimates (Zuckerman et al. 2010, 2003). *Spitzer* observations of the 85 star subsample with *HST* data show that, amongst the 23 metal polluted white dwarfs that are currently accreting, there are two that exhibit detectable infrared excesses: 0843+516 and 1015+161. The co-observed subsample thus translates to approximately 10% of metal-enriched stars exhibiting detectable dust, indicating that about 90% of debris discs escape detection in the infrared. As expected, no infrared excesses are confidently found in the subsample of non-metal bearing degenerates observed with *HST*, strongly supporting the connection between infrared excesses and metal pollution.

Possible reasons for the apparent lack of infrared disc detections are still a matter of debate. The collective data for the known circumstellar discs at hydrogen dominated white dwarfs indicate that the DA degenerates with the highest accretion rates are significantly more likely to host an infrared detectable circumstellar disc (Xu & Jura 2012; Farihi et al. 2009; Jura et al. 2007). The infrared excesses at 0843+516 and 1015+161 confirm this trend, as they both have the highest inferred Si accretion rates amongst the *HST* sample stars (3.6×10^7 g s^{-1} and 5×10^6 g s^{-1} respectively). This is consistent with a picture where white dwarfs accreting at the highest rates require the most massive and highest surface density discs, which are more likely to be detected in the infrared. One possible explanation for the dearth of infrared excesses is that mutual collisions may be enhanced in low surface density discs, and result in the partial or complete destruction of dust grains (Jura et al. 2007). A related possibility is increased, collisional grain destruction due to the impact of additional, relatively small planetesimals on a pre-exiting dust disc (Jura 2008). This may explain the lower frequency of infrared excess detections at older and cooler white dwarfs (Bergfors et al. 2014, see also Section 6), as the depletion of the reservoir of large asteroids for older white dwarfs would imply that smaller planetesimals are primarily accreted. In contrast, this work corroborates the interpretation that the lack of infrared excess detections at a large fraction of metal polluted white dwarfs is largely caused by the small total emitting surface area of dust grains, which implies a very low infrared fractional luminosity and hence undetectability with the current instrumentation. Sections 4.2 and 6 provide evidence supporting this hypothesis.

4.2 Hidden subtle excesses in the DAZ sample

Thanks to the large number of stars observed as part of this *Spitzer* survey, one can investigate the possibility that some DAZ white dwarfs have an infrared excess that is just below the current sensitivity limit. The distribution of excess and deficit infrared fluxes with respect to the model fluxes demonstrates a correlation between subtle infrared excesses and atmospheric metals indicating a population of tenuous circumstellar discs.

The observed excess and deficit fluxes with respect to the model flux at different wavelengths were expressed as a fraction of the photometric and model uncertainties, and were quantified by an excess significance, defined as:

$$\chi = \frac{F_{\rm obs} - F_{\rm model}}{\sqrt{\sigma_{\rm obs}^2 + \sigma_{\rm model}^2}} \qquad (1)$$

where $F_{\rm obs}$ and $F_{\rm model}$ are the observed and photospheric model fluxes respectively, and similarly for the uncertainties, $\sigma_{\rm obs}$ and $\sigma_{\rm model}$.

The excess significance values were derived for each star in the subsample of 85 degenerates that have both *Spitzer* and *HST* observations. Two subgroups were created, one containing non-metal lined (DA) white dwarfs only and one containing degenerates exhibiting atmospheric metals (DAZ) only. All stars that show Si absorption in their spectra – including those whose metals can be explained by radiative levitation alone – were included in the DAZ sample, as these stars have likely accreted circumstellar material recently (Koester et al. 2014). The DA sample consists of 32 stars observed at 3.6 μm and 38 stars at 4.5 μm, while the DAZ sample consists of 34 stars observed at 3.6 μm and 45 stars at 4.5 μm. The differences in the subsample sizes are due to the lack of IRAC observations in channel 1 or 2 for some stars whose data were taken from the *Spitzer* archive. Infrared excesses that have $\chi > 4$ and cases of strong contamination from nearby sources were excluded. The excess significance values were then plotted in separate histograms, for fluxes measured at 3.6 μm and 4.5 μm. The resulting four histograms are shown in Figure 3. It is important to stress that statistically confident excesses are defined for $\chi > 4$, corresponding to a significance level of 4σ. An excess with $1.5 < \chi < 4$ can be defined as a *candidate subtle excess*, which cannot yet be confirmed with confidence. However, one can test the observed distribution of all $\chi < 4$ for each subsample of DA and DAZ stars observed at 3.6 μm and 4.5 μm against expectations.

The number of candidate subtle excesses with $\chi > 1.5$ and their expected values were computed for each of these subsamples, and these are shown in Figure 3. The expected values were inferred assuming no correlation between atmospheric metals and infrared excesses and were computed in the following way. The observed excesses were randomly distributed in two subsamples equal in size to the observed DA

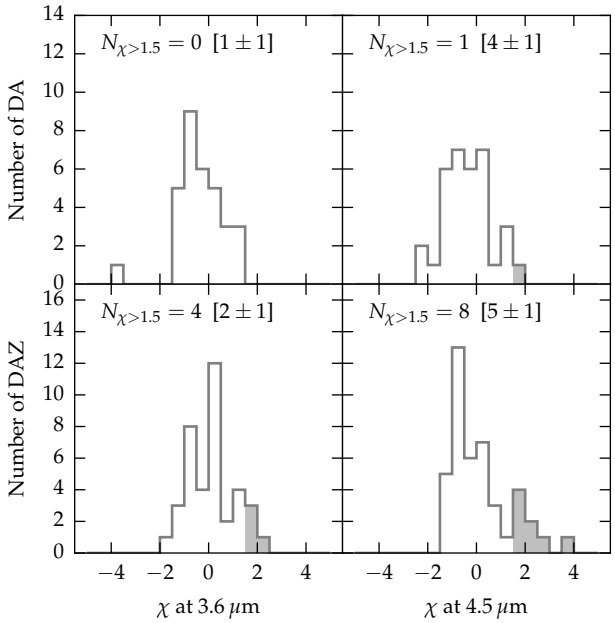

Figure 3. Histograms of excess significance χ for metal lined (DAZ) and non-metal bearing (DA) white dwarfs observed at 3.6 μm and 4.5 μm with IRAC. Stars with $\chi > 1.5$ are highlighted in grey, and their occurrence is given at the top left of each subplot, with expected values in square brackets. Stars with $\chi > 4$ and sources that are heavily contaminated by nearby objects have been excluded.

and DAZ subsamples, at 3.6 and 4.5 μm. This computation was repeated 1000 times, and the average number of stars with $\chi > 1.5$ and its standard deviation were used as estimates.

Interestingly, departure from expectations was found. In the DA sample there is only one candidate excess at 4.5 μm, while the expected number is 1 ± 1 at 3.6 μm and 4 ± 1 at 4.5 μm. In contrast, the bulk of candidate excesses are found in the DAZ sample, where four and eight $\chi > 1.5$ values were found at 3.6 μm and 4.5 μm, while the expected numbers are 2 ± 1 and 5 ± 1 respectively.

This apparent correlation between atmospheric metals and subtle infrared excesses, especially at longer wavelengths, may reinforce the idea that most if not all circumstellar discs at metal polluted white dwarfs harbour dust that emits in the infrared, but its signature is too subtle to be detected with the current instrumentation.

5 COMPARISON WITH PREVIOUS SURVEYS

In this section the frequency of infrared excesses at white dwarfs derived in this work is compared with previous surveys.

Implementing a *ugriz* colour selection valid for $T_{\rm eff} > 8000$ K, Girven et al. (2011) selected 1884 DA white dwarf candidates from the SDSS DR7 catalogue spatially cross-correlated with the UKIDSS catalogue, and found an 0.8% of infrared bright disc candidates. This frequency includes a correction for the contamination of hot stars and subluminous B stars. Amongst the photometrically selected stars, about 1000 white dwarfs were further identified spectroscopically. Restricting this sample to the effective temperature range of the COS/IRAC survey it was found that for $T_{\rm eff} = 17\,000 - 25\,000$ K a fraction of 6.2% have infrared excesses. This frequency is higher than that derived from this *Spitzer* survey, but includes non-discs such as low mass stellar and substellar companions and closely aligned background sources. Similarly, Steele et al. (2011) identified 811 DA white dwarfs with $T_{\rm eff} < 100\,000$ K in common between SDSS DR4, or Sion (1999) catalogues, and UKIDSS. It was found that only three stars have a K-band excess consistent with a debris disc, translating to a nominal frequency of 0.4%. Direct comparison with this work is not possible, due to the disparate effective temperature regimes and the lack of on-line data.

Mid-infrared photometry from the preliminary *Wide-field Infrared Survey Explorer* (*WISE;* Wright et al. 2010) catalogues, cross-correlated with the preliminary SDSS DR7 white dwarf catalogue, resulted in 1527 *WISE* detections and 52 disc candidates (Debes et al. 2011b). The frequency of discs was estimated applying a flux cutoff in the *WISE* photometry, resulting in six disc candidates amongst 395 white dwarfs, and yielding a lower frequency of $1.5\% \pm 0.6\%$. Further analysis of the sample revealed that two of these candidates are spurious, so that a new estimate for the frequency of discs in the brightness limited *WISE* sample is 1% (Barber et al. 2014). This sample had no restriction in effective temperature and included $T_{\rm eff} > 25\,000$ K stars, for which discs have never been confirmed.

These frequencies should be considered with care, as disc candidates often need to be confirmed with additional data. For instance, *Spitzer* observations of six disc candidates from Girven et al. (2011) reveal that only five of the excesses are confirmed at longer wavelengths, and only three are due to dust discs (Farihi et al. 2012). Prior *Spitzer* observations also show that only 50% of dusty white dwarfs show an excess in K-band (Farihi et al. 2010). Lastly, further follow-up of 16 disc candidates in the *WISE* survey (Debes et al. 2011b) revealed that the majority of the detected excesses are due to background contamination (Barber et al. 2014; Wang, Tziamtzis, & Wang 2014), showing that excess photometric fluxes detected with *WISE* need additional confirmation. It is also worth noting that, although many *WISE* disc candidates might be spurious, it is likely that all white dwarfs with bright dust discs have been discovered for the bulk of known white dwarfs (Hoard et al. 2013).

Mullally et al. (2007) presented the first unbiased *Spitzer* surveys of white dwarfs in search of infrared excesses. A brightness limited sample of 135 single stars from Sion (1999) and with $K_s < 15$ mag in 2MASS was selected to be observed at 4.5 and 7.9 μm. Infrared fluxes were successfully measured for 124 of these, and only two showed significant excess due to dust, yielding a frequency of 1.6%. The sample stars have a large temperature range, extending to hot effective temperatures at which solid dust grains rapidly sublimate within the Roche limit of the star. This brightness limited sample was naturally diverse in effective temperature, stellar mass, and atmospheric composition, making it problematic to compare with other surveys.

Barber et al. (2012) report a $4.3^{+2.7}_{-1.2}\%$ frequency of discs at DA white dwarfs but this result contains biases due to 1) the method used to select the statistical sample and 2)

the strategy to detect the discs. A total of 117 single white dwarfs with $T_{\rm eff} = 9500 - 22\,500$ K were selected from the Palomar Green (PG) Survey (Green, Schmidt, & Liebert 1986), but the authors did not provide details on the actual selection. There are in fact 145 single degenerates in the PG catalogue in this temperature range, and all of these stars should have been considered for an unbiased frequency. The frequency reported is also significantly higher than that found by other surveys, especially considering the preliminary K-band excess selection method. As mentioned previously, only about half of known dusty white dwarfs have a K-band excess (Farihi et al. 2010), and this 4.3% frequency represents only a lower limit. This means that excesses that show their signature beyond 2.2 μm have likely been missed. Indeed, one of the stars in the Barber et al. (2012) sample, PG 2328+108, was observed as part of this *Spitzer* survey, and a subtle excess was confidently detected (see Figure 2). It is also worth noting that 2MASS photometry becomes unreliable for sources fainter than $K_s \approx 14$ mag (Farihi 2009; Hoard et al. 2007) and most of their 39 stars with only 2MASS photometry are fainter than this limit. Finally, four previously known dusty white dwarfs (1015+161, 1116+026, 1457–086 and 2326+049) were included in the sample of 117 stars, but were not followed-up photometrically or spectroscopically, and were assumed to have discs a priori. This can introduce a strong bias in disc frequency, as two of these discs (1015+161, 1116+026) do not actually have detectable K-band excess ($J-K = 0.01 \pm 0.10$ and $J-K = 0.08 \pm 0.10$ respectively) and would have been missed if not previously known.

Despite these issues, it is worth trying to derive a robust lower limit for the frequency of detectable discs in the PG catalogue. Considering the infrared excess discovered at 2328+108, together with the other five known infrared excesses detected in the *complete* PG sample of 145 stars with $T_{\rm eff} = 9500 - 22\,500$ K, a lower limit for the disc frequency in this temperature range is 4.1%. Note that other subtle infrared excesses might still be present, as not all 145 stars have *Spitzer* observations. Restricting the range of effective temperatures to $T_{\rm eff} = 17\,000 - 22\,500$ K allows direct comparison with this work. There are 96 stars and five infrared excesses in this temperature range in the sample analysed in this study, translating to a 5.2% frequency. Similarly, there are three infrared excesses amongst 50 stars in the PG sample with $T_{\rm eff} = 17\,000 - 22\,500$ K, yielding a frequency of $\geqslant 6\%$. For comparison, Girven et al. (2011) found a higher fraction of 6.9% K-band excesses in this temperature range, but this frequency does not take into account contaminant sources.

6 THE FRACTIONAL LUMINOSITY OF DUST DISCS

Here it is shown that the distribution of the disc fractional luminosities ($\tau = L_{\rm IR}/L_*$) for the sample of known dusty white dwarfs reinforces the interpretation that a large fraction of circumstellar discs remain undetected in the infrared and may also provide insight into their evolution.

The value of fractional luminosity of all known infrared excesses at cool white dwarfs was estimated in a consistent manner. The photospheric flux was fitted as described in Section 3 and a blackbody distribution was then fitted to the infrared excesses seen in the K-band and the three shortest wavelength IRAC bandpasses. The mid-infrared fluxes were all measured with *Spitzer* IRAC and were obtained from the literature and this work. Although a precise estimate of τ requires detailed modelling of the photospheric and disc flux, the values reported here are estimated to be good to 10%. Independently measured values for 18 discs known as of mid-2010 agree to within 10% (Farihi 2011). Note also that τ is the *observed* fractional luminosity and it does not take into account the disc inclination, which cannot be determined confidently (Section 3.1). The fractional luminosity τ and the blackbody dust temperature $T_{\rm IR}$ for all 35 *Spitzer*

Table 3. Estimated fractional luminosities from thermal continuum for all known white dwarfs exhibiting infrared excess due to dust.

WD	$t_{\rm cool}$ (Myr)	$T_{\rm eff}$ (K)	$T_{\rm IR}$ (K)	τ (%)	Ref.
0106–328	160	16000	1470	0.08	1
0110–565	81	19200	1050	0.15	2
0146+187	418	11500	1120	1.47	3
0246+734†	995	8250	1000	0.31	4
0300–013	189	15200	1200	0.31	5
0307+078	531	10500	1200	0.18	1
0408–041	224	14400	1020	2.94	5
0435+410	116	17500	1250	0.28	2
0735+187	264	13600	1330	1.59	6
0842+231	92	18600	1350	0.60	6
0843+516	29	23900	1310	0.13	7
0956–017	283	13280	1220	2.73	8
1015+161	80	19300	1210	0.17	5
1018+410	45	22390	1210	0.11	9
1041+091	106	17910	1500	0.15	6
1116+026	358	12200	1000	0.48	5
1150–153	314	12800	940	2.02	10
1219+130	350	12300	1250	1.61	8
1225–079	531	10500	300	0.05	1
1226+110	45	22000	1070	0.40	11
1349–230	100	18200	1260	0.33	2
1455+298	1315	7400	400	0.19	12
1457–086	63	20400	1400	0.04	3
1541+651	409	11600	980	1.23	13
1551+175	178	15500	1690	0.19	4
1554+094	37	22800	1100	0.43	8
1615+164	274	13430	1370	1.28	6
1729+371	531	10500	820	2.02	14
1929+011	57	20890	1060	0.19	5
2115–560	653	9700	820	0.84	3
2132+096	301	13000	550	0.11	4
2207+121	122	17300	1100	0.74	7
2221–165	588	10100	950	0.67	1
2326+049	409	11600	1060	2.87	12
2328+107	37	21000	2000	0.05	9

† Needs to be confirmed.

References:
(1) Farihi et al. (2010) (2) Girven et al. (2012) (3) Farihi et al. (2009) (4) Bergfors et al. (2014) (5) Jura et al. (2007) (6) Brinkworth et al. (2012) (7) Xu & Jura (2012) (8) Zuckerman et al. (2003); Farihi et al. (2012) (9) this work; (10) Jura et al. (2009) (11) Brinkworth et al. (2009) (12) Farihi et al. (2008b) (13) Barber et al. (2012) (14) Jura et al. (2007)

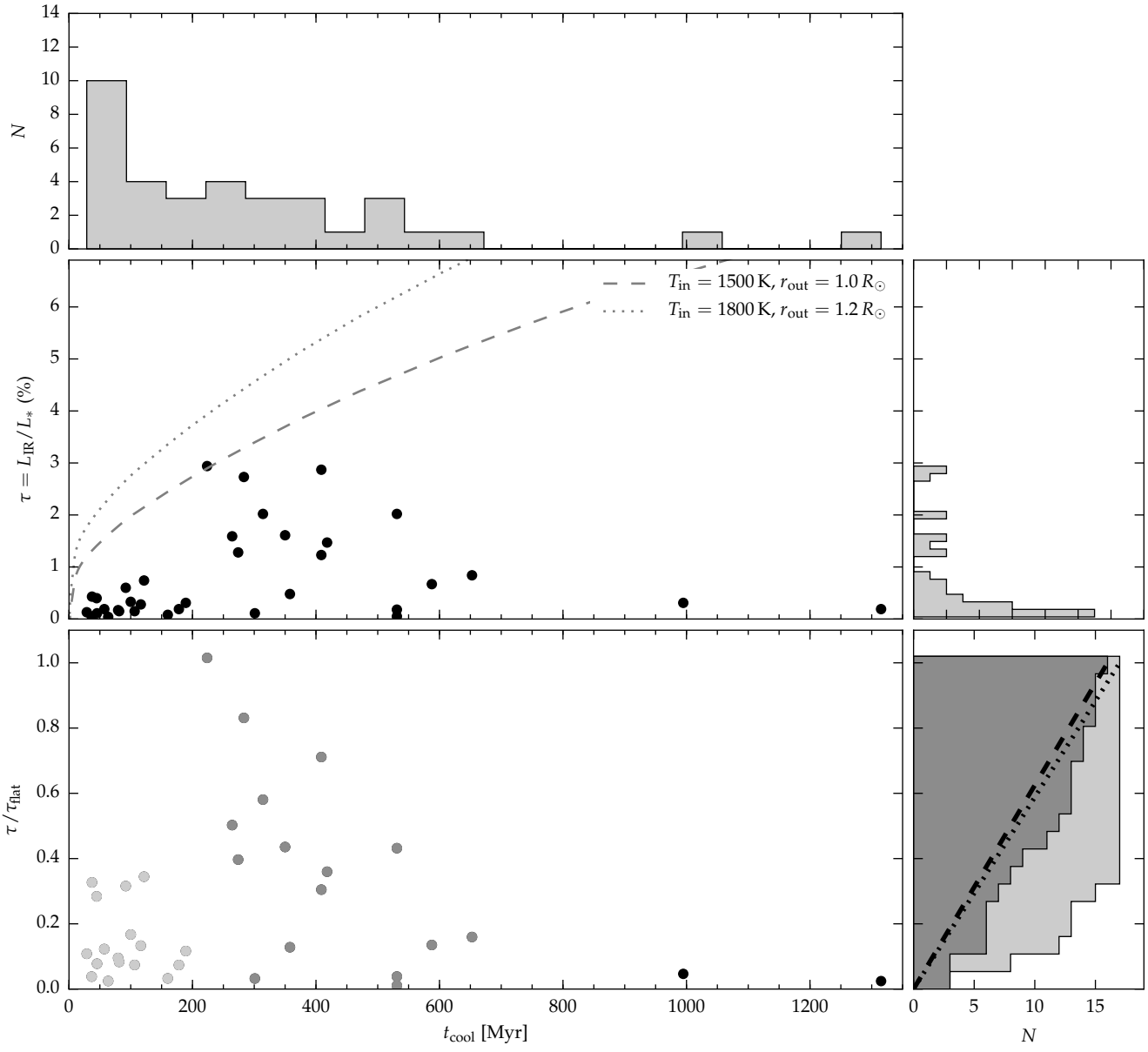

Figure 4. Fractional disc luminosities ($\tau = L_{\rm IR}/L_*$) for all known white dwarfs with detected dust discs. The central panel shows the value of τ as a function of cooling age for $\log g = 8$. The two lines lines show the predicted fractional luminosity for a face on, opaque flat disc with radial extent given by assuming dust grains persist up to 1500 and 1800 K and extend up to $1.0\,R_\odot$ and $1.2\,R_\odot$. The dotted line is for $T_{\rm in} = 1500\,{\rm K}$ and $r_{\rm out} = 1.0\,R_\odot$, while the dashed line is for $T_{\rm in} = 1800\,{\rm K}$ and $r_{\rm out} = 1.2\,R_\odot$. The top panel shows the histogram of the number of infrared excesses as a function of cooling age, while the right panel shows the histogram of τ with 20 bins between 0 and 3%. The bottom panel shows the ratio between the infrared fractional luminosity of all known dusty white dwarfs and the predicted maximum fractional luminosity for a flat, passive disc, assuming $T_{\rm in} = 1500\,{\rm K}$ and $r_{\rm out} = 1.0\,R_\odot$. The light grey symbols have $t_{\rm cool} < 200\,{\rm Myr}$, while the dark grey symbols have $200\,{\rm Myr} < t_{\rm cool} < 700\,{\rm Myr}$. The bottom-right panel shows the cumulative histograms of $\tau/\tau_{\rm flat}$ for the light and dark grey target subsets, and the expected distributions for random inclinations are shown as dotted and dashed lines respectively.

detected white dwarfs with infrared excesses are listed in Table 3. The measured values of τ and their distribution are also plotted in Figure 4.

6.1 An undetected population of subtle excesses

The right hand histogram of the middle panel of Figure 4 shows the distribution of τ, with 20 bins between 0% and 3%. It can be seen that the distribution rises sharply at the smallest fractional luminosities indicating that the majority of circumstellar discs are subtle. This suggests that many discs might have a fractional luminosity that is below the sensitivity limits of the current instrumentation and therefore escape detection.

Together with the likely presence of several additional subtle excesses seen in this *Spitzer* sample (see Section 4.2), the distribution of τ points to a large population of subtle excesses, suggesting that most if not all, currently accreting white dwarfs with metals have circumstellar dust. This significant population of dust discs are not detectable with current facilities, likely due to low surface areas and optical depth.

6.2 Narrow rings at young white dwarfs

The central panel of Figure 4 shows τ as a function of cooling age. The two lines represent the value of the maximum fractional disc luminosity $\tau_{\rm flat}$ for a flat disc model (Jura 2003) with a face-on configuration. This value was calculated assuming that the dust occupies all the space available between the distance from the star at which dust grains rapidly sublimate and the stellar Roche limit. The two lines correspond to two different assumptions about the maximum disc extent. The dotted line assumes that silicates rapidly sublimate at $T_{\rm in} = 1800\,{\rm K}$ and the stellar Roche limit is $r_{\rm out} = 1.2\,R_{\odot}$, while the dashed line assumes $T_{\rm in} = 1500\,{\rm K}$ and $r_{\rm out} = 1.0\,R_{\odot}$.

From the central panel it can be seen that infrared excesses have so far only been detected at white dwarfs older than $\approx 25\,{\rm Myr}$, and with corresponding $T_{\rm eff} \lesssim 25\,000\,{\rm K}$. This is somewhat expected, as at higher stellar temperatures, any disrupted asteroids debris will evaporate relatively quickly, so that their detection is less likely. However, the calculations done here and shown in the plot indicate that optically thick discs may exist at higher effective temperatures and cooling ages. Such discs would likely evolve more rapidly (Rafikov 2011), and have a higher gas to dust ratios from sublimation prior to settling into optically thick rings.

As the white dwarf cools below 25 000 K the distance at which silicates rapidly sublimate decreases. Hence, the area available for dust grains increases, so that the disc luminosity should increase as well. *However, the expected increase assuming that discs are fully extended (shown by the two lines in the central panel of Figure 4), is not seen in the observed fractional luminosities.* Between 25 Myr and 200 Myr there are 17 dusty white dwarfs, all with fractional luminosities significantly less than the maximum value allowed for flat discs. This suggests that, at these young white dwarfs, large and extended discs do not form, or only persist for timescales significantly shorter than the disc lifetime.

This finding can be better explored and tested in the bottom-left panel of Figure 4, showing the ratio $\tau/\tau_{\rm flat}$ for $T_{\rm in} = 1500\,{\rm K}$ and $r_{\rm out} = 1.0\,R_{\odot}$ as a function of cooling age. Supposing that discs are fully extended, and assuming random inclinations, the distribution of $\tau/\tau_{\rm flat}$ should be uniform between zero and one. However, this does not seem to be true, especially for white dwarfs younger than 200 Myr and older than 700 Myr. To better explore if discs have different radial extents at different ages it is useful to consider three cooling age ranges separately, for $t_{\rm cool} < 200\,{\rm Myr}$ (light grey symbols), for $200\,{\rm Myr} < t_{\rm cool} < 700\,{\rm Myr}$ (dark grey symbols), and for $t_{\rm cool} > 700\,{\rm Myr}$. It can be seen that:

1) At $t_{\rm cool} < 200\,{\rm Myr}$, the $\tau/\tau_{\rm flat}$ values are all below 0.4, clearly demonstrating that inclination is not the only parameter influencing the distribution. A Kolmogorov–Smirnov (KS) test confirms this, resulting in a probability of 2×10^{-7} that the observed distribution is uniform in $\tau/\tau_{\rm flat}$. As any observational bias would favour the detection of discs with lower inclinations and correspondingly higher fractional luminosities, this indicates that the observed discs must be relatively narrow at these young cooling ages.

2) Between $200\,{\rm Myr} < t_{\rm cool} < 700\,{\rm Myr}$ there is a notable increase in the observed fractional luminosities, with the brightest ($\tau \approx 3\%$) disc modelled as face on at 0408–041 (GD 56). In this range of cooling ages, a KS test reveals that the distribution of $\tau/\tau_{\rm flat}$ is uniform with a probability of only 0.07, again indicating that a second parameter shapes the distribution, namely the disc radial extent. While not as striking as for the youngest cooling ages, this group likely contains several relatively narrow discs, as indicated by the cumulative distribution at smaller $\tau/\tau_{\rm flat}$ values.

3) Lastly, at $t_{\rm cool} > 700\,{\rm Myr}$ there are only two detected discs with relatively low fractional luminosities ($\tau < 0.3\%, \tau/\tau_{\rm flat} < 0.05$). The small τ values of these discs, together with the decreasing frequency of detections seen at older white dwarfs (top histogram of Figure 4), suggest that the number of large asteroid disruptions per time bin may be decreasing and hence also the fraction of detectable infrared excesses (Bergfors et al. 2014). However, it is interesting to note that the inferred metal accretion rates do not show a decreasing trend with cooling age (Koester et al. 2014), indicating that circumstellar material is present at older stars. This could be explained by the accretion of smaller asteroids, which can still provide continuous accretion, but are less likely to produce detectable amounts of dust (Wyatt et al. 2014).

6.3 Possible disc evolution scenarios

Interestingly, the existence of narrow rings is predicted by global models of white dwarf disc evolution. In general, the outer radii of flat and optically thick discs will rapidly decrease due to Poynting-Robertson (PR) drag. Specifically, for a range of initial, realistic surface density distributions, PR drag is significantly more efficient per unit mass on the outermost (and innermost) disc regions where grain density and optical depth is lowest. Solids are quickly gathered inward until they result in a region of moderate optical depth (Metzger, Rafikov, & Bochkarev 2012; Bochkarev & Rafikov 2011), giving rise to a sharp outer edge.

This edge forms rapidly, and marches appreciably in-

ward within a few to several hundred PR drag timescales (Bochkarev & Rafikov 2011), which can be as short as years for typical dusty white dwarfs and 1 μm dust at 1 $R_\odot$. The rate at which the outer edge migrates inward will be ultimately set by the dominant grain size, as the rate scales linearly with particle size and can be a factor of 1000 longer for centimetre vs. micron sizes. Stellar luminosity plays a smaller role, varying by less than a factor of 20 between typical 10 000 K and 20 000 K white dwarfs (Fontaine et al. 2001). Thus, if this mechanism is responsible for sculpting narrow rings, their radial extents as a function of white dwarf cooling age and luminosity may broadly constrain typical particle sizes.

The transition in disc brightness between the $t_{\rm cool} < 200$ Myr and 200 Myr $< t_{\rm cool} < 700$ Myr cooling age ranges appears relatively abrupt, however, and it is not clear that a change in stellar luminosity (and PR drag timescale) alone can account for the difference between the two populations. It is perhaps tempting to interpret the brighter and presumably larger discs at 200 Myr $< t_{\rm cool} < 700$ Myr as evidence of disc spreading, but the viscous timescale among particulates, for any reasonable particle size, is orders of magnitude insufficient and thus highly unlikely to have an effect on disc evolution (Metzger et al. 2012; Farihi et al. 2008b).

A distinct possibility for the narrowing of rings is disc truncation by impact. Theoretical models show that post-main sequence dynamical instabilities arise near $\sim$ 10 Myr, then peak around $\sim$ 100 Myr, decreasing towards later times (Veras et al. 2013; Mustill, Veras, & Villaver 2014). This suggests that impacts on pre-existing discs by additional, perturbed and tidally shredded asteroids would be most prevalent among the $t_{\rm cool} < 200$ Myr disc sample. Disc impacts would have the favourable characteristic that they should occur preferentially at larger orbital radii, thus typically creating outwardly truncated discs. The impactor fragments would destroy dust masses comparable to their initial, intact masses, creating gas that would quickly dissipate (Jura 2008). Interestingly, the recently observed drop in infrared luminosity from the dusty white dwarf SDSS J095904.69−020047.6, and the disappearance of metallic gas emission lines from the similarly dusty and polluted star SDSS J161717.04+162022.4, may represent such impact events (Xu & Jura 2014; Wilson et al. 2014).

Because viscous spreading is inefficient (see above), discs will not grow outward significantly during their lifetime, and the narrower discs might be the result of initial conditions; specifically, smaller disrupted parent bodies. However, assuming the same overall disc properties, flat configurations and random inclinations, the average disc mass should correlate with τ over each population, implying parent body masses all similar to within a factor of roughly 50. This would require relatively fine-tuned mass influxes per unit time in the post-main sequence, including a subtle change around 300 Myr to include slightly larger disruptions. Taken together, this seems unlikely to account for the disc brightness differences among the two cooling age ranges.

In summary, while none of the above mechanisms appears to be without possible drawbacks, the clear observational difference in disc populations demands a closer look with formation and evolutionary modelling. Insufficient data could be masking a more gradual change in the fractional disc luminosities that would favour the edge migration scenario, for example. The detection of a larger number of discs, especially those producing subtle excesses, would improve the statistics and reduce the possibilities.

7 NOTES ON INDIVIDUAL TARGETS

7.1 Sample stars with infrared excesses

0843+516 and 1015+161. These are two metal polluted white dwarfs (Gänsicke et al. 2012) with known infrared excesses (Xu & Jura 2012; Jura et al. 2007). The excesses at 7.9 μm lay significantly above the predicted fluxes of both disc models (Figure 2), likely due to the presence of a strong silicate emission feature.

1018+410. The infrared excess detected at this star is reported here for the first time. There is no reliable near-infrared photometry available for this star, and the 2MASS catalogue only reports $H = 16.7 \pm 0.1$ mag. However, *ugriz* photometry is available from SDSS and the photospheric level of the white dwarf can be well constrained. This degenerate was not observed in the complementary *HST* survey, and there are no high-resolution optical spectra available. Follow-up should confirm that this is a DAZ white dwarf.

1457–086. This is a known metal polluted white dwarf (Koester et al. 2005) that was found to host a narrow dust ring with high inclination and radial extent of only 0.01 $R_\odot$ (Farihi et al. 2009). The fit to the excess emission with both a narrow and highly inclined disc model show that the optical fluxes might be overestimated and 15% error bars were assumed to obtain a satisfactory fit. The star was not observed in the complementary *HST* survey and additional optical photometry may better constrain the photospheric flux.

2328+107. With a fractional luminosity of only 0.1% this infrared excess, reported here for the first time, joins an expanding list of attenuated discs (Bergfors et al. 2014; Farihi et al. 2010). Both *JHK* and *ugriz* photometry are available from the 2MASS and SDSS online catalogues and allow to constrain the photospheric level confidently. This degenerate was not observed in the *HST* survey and high-resolution spectra are not yet available but should reveal the presence of metals.

7.2 The infrared excess at 1929+012

This star, also known as GALEX 1931, is a metal polluted white dwarf (Vennes et al. 2010) with a known infrared excess (Gänsicke et al. 2012; Melis et al. 2011; Debes et al. 2011a), included in the *Spitzer* Program as an ancillary target. Photometry from *WISE* revealed infrared excess consistent with emission from a dust disc (Debes et al. 2011a), while ground-based photometry out to *L*-band indicated significant contamination from background sources in the *WISE* data (Melis et al. 2011). The *Spitzer* IRAC 3.6 and 4.5 μm photometry of GALEX 1931 confirms the excess emission but is heavily blended with two nearby sources, as shown by the $J_s H K_s L'$ higher resolution images (Melis et al. 2011). Despite the success in extracting most of the flux, the relatively low spatial resolution of IRAC implies likely contamination in the derived fluxes. Therefore, 10% error bars

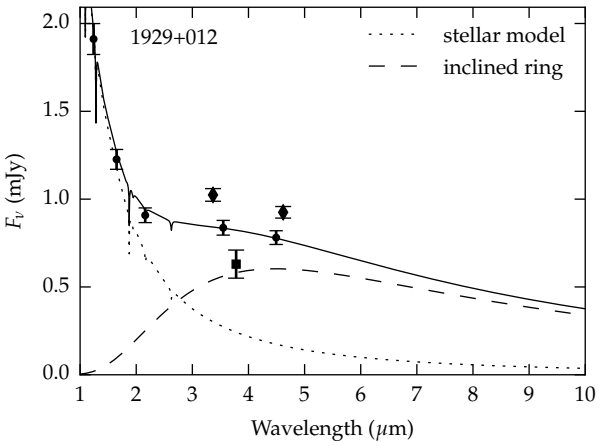

Figure 5. SED and disc model for the ancillary target 1929+012. Fluxes from *WISE* All-Sky catalogue are plotted as diamond symbols and fluxes from ISAAC L' as square symbols. Circles symbols represent 2MASS and IRAC fluxes.

are conservatively assumed in the resulting photometry. Figure 5 shows the SED of 1929+012, including IRAC, ISAAC L' (Melis et al. 2011), and *WISE* All-Sky photometry. A fiducial disc model is also plotted. It can be seen that the IRAC fluxes are somewhat lower than the *WISE* values, but also higher than the ground-based L-band flux. These data indicate mild contamination is likely in the IRAC data and strong contamination is present in *WISE*.

8 SUMMARY AND CONCLUSION

Spitzer observations of an unbiased sample of 134 DA white dwarfs yield a disc frequency near 4% in the effective temperature range $T_{\rm eff} = 17\,000\,{\rm K} - 25\,000\,{\rm K}$. Complementary *HST* observations of 85 sample stars reveal that a much larger fraction of at least 27% host circumstellar material, indicating that about 90% of the discs remain undetected in the infrared.

Possible reasons for the lack of infrared detections were investigated. The distribution of observed fluxes compared to photospheric models at 3.6 and 4.5 μm for the subsamples with and without metals point to a population of excesses too subtle to currently confirm. Future observations, for example with *JWST* using spectroscopy, have the potential to confirm the presence of faint dust discs.

The distribution of the fractional disc luminosities of all known dusty white dwarfs also points towards a hidden population of subtle discs. In addition, this distribution indicates that the disc population evolves over time. Only relatively narrow rings are found at $t_{\rm cool} \lesssim 200\,{\rm Myr}$, while relatively extended discs, filling the majority of the space available between the distance at which silicates rapidly sublimate and the stellar Roche limit, occur only after a few hundred Myr. A marked decrease in the observed fractional disc luminosities, as well as a decrease in the frequency of detections towards cooler ages, is seen after this peak, suggesting that the number of large asteroids might be gradually depleted.

This study strongly reinforces the hypothesis that most if not all metal-enriched white dwarfs harbour circumstellar dust, but the majority remain unseen due to low surface area and the sensitivity limits of current instrumentation.

ACKNOWLEDGMENTS

The authors thank the anonymous referee for suggestions that improved the manuscript. The authors acknowledge Tom Marsh and Mark Hollands for discussions on disc geometry, and Giuseppe Morello and Ingo Waldmann for discussions on statistics. This work is based on observations made with the *Spitzer Space Telescope*, which is operated by the Jet Propulsion Laboratory, Caltech, under NASA contracts 1407 and 960785. The following databases were used in the process of this research: the Sloan Digital Sky Survey, which is managed by the Astrophysical Research Consortium for the Participating Institutions (http://www.sdss.org/); the Two Micron All Sky Survey, which is a joint project of the University of Massachusetts and IPAC/Caltech, funded by NASA and the NSF; the Deep Near-Infrared Survey of the southern sky, which has been partly funded by the SCIENCE and the HCM plans of the European Commission; the AAVSO Photometric All-Sky Survey, funded by the Robert Martin Ayers Sciences Fund. This research has made use of the VizieR catalogue access tool and the SIMBAD database operated at CDS, Strasbourg, France. MR, JF, and CB collectively acknowledge support from the STFC; JF via an Ernest Rutherford Fellowship. The research leading to these results has received funding from the European Research Council under the EU 7th Framework Programme (FP/2007–2013)/ERC Grant Agreement n. 320964 (WDTracer).

REFERENCES

Adams E. R., Seager S., Elkins-Tanton L., 2008, ApJ, 673, 1160
Ahn C. P. et al., 2012, ApJS, 203, 21
Alcock C., Fristrom C. C., Siegelman R., 1986, ApJ, 302, 462
Barber S. D., Kilic M., Brown W. R., Gianninas A., 2014, ApJ, 786, 77
Barber S. D., Patterson A. J., Kilic M., Leggett S. K., Dufour P., Bloom J. S., Starr D. L., 2012, ApJ, 760, 26
Becklin E. E., Farihi J., Jura M., Song I., Weinberger A. J., Zuckerman B., 2005, ApJ, 632, L119
Bergfors C., Farihi J., Dufour P., Rocchetto M., 2014, MNRAS, 444, 2147
Bochkarev K. V., Rafikov R. R., 2011, ApJ, 741, 36
Bonsor A., Mustill A. J., Wyatt M. C., 2011, MNRAS, 414, 930
Brinkworth C. S., Gänsicke B. T., Girven J. M., Hoard D. W., Marsh T. R., Parsons S. G., Koester D., 2012, ApJ, 750, 86
Brinkworth C. S., Gänsicke B. T., Marsh T. R., Hoard D. W., Tappert C., 2009, ApJ, 696, 1402
Byrd R. H., Lu P., Nocedal J., Zhu C., 1995, SIAM Journal on Scientific Computing
Chiang E. I., Goldreich P., 1997, ApJ, 490, 368

Debes J. H., Hoard D. W., Kilic M., Wachter S., Leisawitz D. T., Cohen M., Kirkpatrick J. A., Griffith R. L., 2011a, ApJ, 729, 4
Debes J. H., Hoard D. W., Wachter S., Leisawitz D. T., Cohen M., 2011b, ApJS, 197, 38
Debes J. H., Kilic M., Faedi F., Shkolnik E. L., Lopez-Morales M., Weinberger A. J., Slesnick C., West R. G., 2012a, ApJ, 754, 59
Debes J. H., Sigurdsson S., 2002, ApJ, 572, 556
Debes J. H., Sigurdsson S., Hansen B., 2007, AJ, 134, 1662
Debes J. H., Walsh K. J., Stark C., 2012b, ApJ, 747, 148
Desharnais S., Wesemael F., Chayer P., Kruk J. W., Saffer R. A., 2008, ApJ, 672, 540
Dufour P. et al., 2007, ApJ, 663, 1291
Dupuis J., Fontaine G., Pelletier C., Wesemael F., 1992, ApJS, 82, 505
Dupuis J., Fontaine G., Pelletier C., Wesemael F., 1993a, ApJS, 84, 73
Dupuis J., Fontaine G., Wesemael F., 1993b, ApJS, 87, 345
Epchtein N. et al., 1999, A&A, 349, 236
Farihi J., 2009, MNRAS, 398, 2091
Farihi J., 2011, White Dwarf Atmospheres and Circumstellar Environments, 117
Farihi J., Becklin E. E., Zuckerman B., 2008a, ApJ, 681, 1470
Farihi J., Gänsicke B. T., Koester D., 2013, Science, 342, 218
Farihi J., Gänsicke B. T., Steele P. R., Girven J. M., Burleigh M. R., Koester D., 2012, MNRAS, 421, 1635
Farihi J., Jura M., Zuckerman B., 2009, ApJ, 694, 805
Farihi J., Jura M., Zuckerman B., 2010, ApJ, 714, 1386
Farihi J., Zuckerman B., Becklin E. E., 2008b, ApJ, 674, 431
Fazio G. G. et al., 2004, ApJS, 154, 10
Fontaine G., Brassard P., Bergeron P., 2001, The Publications of the Astronomical Society of the Pacific, 113, 409
Fontaine G., Michaud G., 1979, ApJ, 231, 826
Frewen S. F. N., Hansen B. M. S., 2014, MNRAS, 439, 2442
Gänsicke B. T., Koester D., Farihi J., Girven J. M., Parsons S. G., 2012, MNRAS, 424, 333
Gänsicke B. T., Marsh T. R., Southworth J., Rebassa-Mansergas A., 2006, Science, 314, 1908
Girven J. M., Brinkworth C. S., Farihi J., Gänsicke B. T., Hoard D. W., Marsh T. R., Koester D., 2012, ApJ, 749, 154
Girven J. M., Gänsicke B. T., Steeghs D., Koester D., 2011, MNRAS, 417, 1210
Green R. F., Schmidt M., Liebert J., 1986, ApJS, 61, 305
Grillmair C. J., Charbonneau D., Burrows A., Stauffer J. R., Meadows V., Levine D., 2007, ApJ, 658, L115
Henden A. A., Welch D. L., Terrell D., Levine S. E., 2009, American Astronomical Society, 214
Hoard D. W., Debes J. H., Wachter S., Leisawitz D. T., Cohen M., 2013, ApJ, 770, 21
Hoard D. W., Wachter S., Gibiansky M., 2007, AJ, 134, 26
Holberg J. B., Bergeron P., 2006, AJ, 132, 1221
Hunt L. K., Mannucci F., Testi L., Migliorini S., Stanga R. M., Baffa C., Lisi F., Vanzi L., 1998, AJ, 115, 2594
Jura M., 2003, ApJ, 584, L91
Jura M., 2008, AJ, 135, 1785
Jura M., Farihi J., Zuckerman B., 2007, ApJ, 663, 1285
Jura M., Farihi J., Zuckerman B., 2009, AJ, 137, 3191
Kalirai J. S., Hansen B. M. S., Kelson D. D., Reitzel D. B., Rich R. M., Richer H. B., 2008, ApJ, 676, 594
Klein B., Jura M., Koester D., Zuckerman B., Melis C., 2010, ApJ, 709, 950
Koester D., 2010, Memorie della Societa Astronomica Italiana, 81, 921
Koester D., Gänsicke B. T., Farihi J., 2014, A&A, 566, 34
Koester D., Rollenhagen K., Napiwotzki R., Voss B., Christlieb N., Homeier D., Reimers D., 2005, A&A, 432, 1025
Koester D., Voss B., Napiwotzki R., Christlieb N., Homeier D., Lisker T., Reimers D., Heber U., 2009, A&A, 505, 441
Lawrence A. et al., 2007, MNRAS, 379, 1599
Liebert J., Bergeron P., Holberg J. B., 2005, ApJS, 156, 47
Lodders K., 2003, ApJ, 591, 1220
Makovoz D., Roby T., Khan I., Booth H., 2006, Advanced Software and Control for Astronomy. Edited by Lewis, 6274, 10
Manchado A. et al., 1998, Proc. SPIE Vol. 3354, 3354, 448
Melis C., Farihi J., Dufour P., Zuckerman B., Burgasser A. J., Bergeron P., Bochanski J. J., Simcoe R., 2011, ApJ, 732, 90
Metzger B. D., Rafikov R. R., Bochkarev K. V., 2012, Monthly Notices of the Royal Astronomical Society, 423, 505
Moorwood A., Cuby J. G., Lidman C., 1998, The Messenger, 91, 9
Mullally F., Kilic M., Reach W. T., Kuchner M. J., von Hippel T., Burrows A., Winget D. E., 2007, ApJS, 171, 206
Mustill A. J., Veras D., Villaver E., 2014, MNRAS, 437, 1404
Paquette C., Pelletier C., Fontaine G., Michaud G., 1986, ApJS, 61, 197
Rafikov R. R., 2011, MNRAS, 416, L55
Rafikov R. R., 2012, ApJ, 760, 123
Rafikov R. R., De Colle F., 2006, ApJ, 646, 275
Reach W. T., Kuchner M. J., von Hippel T., Burrows A., Mullally F., Kilic M., Winget D. E., 2005, ApJ, 635, L161
Reach W. T., Lisse C., von Hippel T., Mullally F., 2009, ApJ, 693, 697
Sion E. M., 1999, ApJS, 121, 1
Skrutskie M. F. et al., 2006, AJ, 131, 1163
Steele P. R., Burleigh M. R., Dobbie P. D., Jameson R. F., Barstow M. A., 2011, MNRAS, 416, 2768
Tinetti G. et al., 2007, Nature, 448, 169
Valencia D., Sasselov D. D., O'Connell R. J., 2007, ApJ, 665, 1413
Vennes S., Kawka A., Németh P., 2010, MNRAS, 404, L40
Veras D., Leinhardt Z. M., Bonsor A., Gaensicke B. T., 2014, arXiv, 2493
Veras D., Mustill A. J., Bonsor A., Wyatt M. C., 2013, MNRAS, 431, 1686
von Hippel T., Kuchner M. J., Kilic M., Mullally F., Reach W. T., 2007, ApJ, 662, 544
Wang Z., Tziamtzis A., Wang X., 2014, ApJ, 782, 20
Werner M. W. et al., 2004, ApJS, 154, 1
Wilson D. J., Gänsicke B. T., Koester D., Raddi R., Breedt E., Southworth J., Parsons S. G. 2014, MNRAS, 445, 1878
Wolff B., Koester D., Liebert J., 2002, A&A, 385, 995
Wright E. L. et al., 2010, AJ, 140, 1868

Wyatt M. C., Farihi J., Pringle J. E., Bonsor A., 2014, Monthly Notices of the Royal Astronomical Society, 439, 3371
Xu S., Jura M., 2012, ApJ, 745, 88
Xu S., Jura M., 2014, The Astrophysical Journal Letters, 792, L39
Zuckerman B., Becklin E. E., 1987, Nature, 330, 138
Zuckerman B., Koester D., Melis C., Hansen B. M., Jura M., 2007, ApJ, 671, 872
Zuckerman B., Koester D., Reid I. N., Hünsch M., 2003, ApJ, 596, 477
Zuckerman B., Melis C., Klein B., Koester D., Jura M., 2010, ApJ, 722, 725

APPENDIX A: SUPPLEMENTARY MATERIAL

Table A1: Stellar parameters and flux determinations for the science targets

WD	$T_{\rm eff}$ (K)	$\log g$ [$\log(\mathrm{cm\,s^{-2}})$]	V (mag)	$M_{\rm wd}$ ($M_\odot$)	$M_{\rm ms}$ ($M_\odot$)	$\log(t_{\rm cool})$ [$\log(\mathrm{yr})$]	$F_{3.6\,\mu\mathrm{m}}$ (μJy)	$F_{4.5\,\mu\mathrm{m}}$ (μJy)	$F_{5.7\,\mu\mathrm{m}}$ (μJy)	$F_{7.9\,\mu\mathrm{m}}$ (μJy)
0000+171	20 210	7.99	15.81	0.62	2.07	7.81	64 ± 3	44 ± 2	...	...
0013–241	18 530	7.90	15.38	0.56	1.56	7.90	103 ± 5	66 ± 3	...	...
0018–339	20 630	7.84	14.64	0.54	1.36	7.65	199 ± 10	119 ± 6	...	...
0028–474	17 390	7.65	15.15	0.44	...	7.87	166 ± 8	104 ± 5	...	...
0047–524	18 810	7.73	14.23	0.48	0.83	7.77	...	189 ± 9	...	65 ± 3
0048+202	20 360	7.89	15.38	0.57	1.57	7.72	101 ± 5	64 ± 3	...	...
0048–544	17 870	7.98	15.16	0.61	1.94	8.02	125 ± 6	81 ± 4	...	...
0059+257	21 370	8.04	15.90	0.65	2.35	7.75	68 ± 3	43 ± 2	...	...
0102+095	24 770	7.93	14.44	0.60	1.86	7.28	217 ± 10	146 ± 7	...	...
0110–139	24 690	7.99	15.75	0.63	2.16	7.36	60 ± 3	38 ± 2	...	...
0114–605	24 690	7.75	15.11	0.51	1.08	7.17	112 ± 5	75 ± 3	...	...
0124–257	23 040	7.79	16.18	0.52	1.18	7.35	36 ± 2	25 ± 1	...	...
0127+270	24 870	7.83	15.90	0.55	1.40	7.18	45 ± 2	28 ± 1	...	...
0129–205	19 950	7.88	15.30	0.56	1.54	7.75	103 ± 5	68 ± 3	...	...
0140–392	21 810	7.92	14.35	0.58	1.74	7.59	254 ± 12	165 ± 8	...	...
0155+069	22 010	7.67	15.47	0.47	0.66	7.39	108 ± 5	68 ± 3	...	...
0200+248	23 280	7.86	15.71	0.56	1.50	7.37	105 ± 11	71 ± 7	...	...
0201–052	24 630	7.64	...	0.46	0.62	7.19	41 ± 2	27 ± 1	...	...
0221–055	24 750	7.72	16.22	0.50	0.94	7.16	61 ± 3	42 ± 2	...	...
0222–265	23 200	7.91	15.68	0.58	1.74	7.43	76 ± 4	51 ± 2	...	...
0227+050	19 340	7.76	12.80	0.50	0.97	7.73	...	775 ± 38	...	255 ± 12
0229+270	24 160	7.90	15.52	0.58	1.71	7.31	79 ± 4	51 ± 2	...	...
0231–054	17 310	8.45	14.31	0.90	4.60	8.42	...	236 ± 11	...	71 ± 3
0242–174	20 660	7.85	15.38	0.55	1.41	7.66	96 ± 4	62 ± 3	...	...
0300–232	22 370	8.39	15.68	0.86	4.32	8.04	72 ± 3	44 ± 2	...	...
0307+149	21 410	7.91	15.38	0.58	1.69	7.62	112 ± 5	71 ± 3	...	...
0308+188	18 450	7.72	14.19	0.48	0.79	7.80	319 ± 16	204 ± 10	...	...
0308–230	23 570	8.54	15.08	0.96	5.18	8.10	108 ± 5	69 ± 3	...	...
0331+226	21 450	7.78	15.28	0.52	1.12	7.52	110 ± 5	70 ± 3	...	...
0341+021	22 150	7.27	15.41	0.33	...	7.27	101 ± 5	60 ± 3	...	...
0349–256	20 970	7.91	15.67	0.58	1.67	7.67	71 ± 3	47 ± 2	...	...
0352+018	22 110	7.80	15.57	0.52	1.19	7.46	79 ± 4	50 ± 2	...	...
0358–514	23 380	7.93	15.72	0.59	1.82	7.43	69 ± 3	47 ± 2	...	...
0403–414	22 700	7.94	16.35	0.60	1.85	7.51	41 ± 2	26 ± 1	...	...
0410+117	21 070	7.84	13.91	0.54	1.37	7.60	...	246 ± 12	...	63 ± 3
0414–406	20 940	8.00	16.13	0.63	2.13	7.75	47 ± 2	29 ± 1	...	...
0416–105	24 850	7.92	15.37	0.59	1.80	7.26	87 ± 4	52 ± 2	...	...
0418–103	23 390	8.29	15.68	0.80	3.76	7.87	70 ± 3	44 ± 2	...	...
0421+162	19 620	8.03	14.29	0.64	2.23	7.89	275 ± 13	171 ± 8	115 ± 6	60 ± 5
0431+126	21 370	7.97	14.23	0.61	1.98	7.68	...	177 ± 8	...	34 ± 7
0452–347	21 210	7.84	16.13	0.54	1.36	7.59	57 ± 3	36 ± 1	...	...
0455–532	24 430	7.55	...	0.43	...	7.22	30 ± 1	17 ± 1	...	...
0507+045.1	20 840	7.90	14.22	0.57	1.62	7.67	...	206 ± 10	...	136 ± 12
0843+516	23 870	7.90	16.04	0.58	1.70	7.35	136 ± 6	137 ± 7	103 ± 5	162 ± 9
0854+404	22 250	7.91	14.81	0.58	1.71	7.53	156 ± 7	97 ± 4	...	...
0859–039	23 730	7.79	13.19	0.53	1.21	7.28	703 ± 35	435 ± 21	...	...
0920+363	24 060	7.63	16.07	0.46	0.58	7.22	56 ± 2	35 ± 1	...	...
0933+025	22 360	8.04	15.93	0.65	2.37	7.66	3569 ± 178	2450 ± 122	...	...
0938+550	18 530	8.10	14.79	0.68	2.62	8.04	197 ± 9	123 ± 6	...	...
0944+192	17 440	7.88	14.51	0.55	1.47	8.00	246 ± 12	159 ± 8	...	...
0947+325	22 060	8.31	15.50	0.82	3.87	7.98	87 ± 4	57 ± 2	...	...
0954+697	21 420	7.91	15.96	0.58	1.69	7.62	63 ± 3	44 ± 2	...	...
1003–023	20 610	7.89	15.27	0.57	1.58	7.69	120 ± 6	73 ± 3	...	...
1005+642	19 660	7.93	13.69	0.58	1.75	7.82	460 ± 23	291 ± 14	...	...
1012–008	23 200	8.07	15.59	0.67	2.57	7.62	79 ± 4	49 ± 2	...	...
1013+256	21 990	8.00	16.32	0.63	2.15	7.65	41 ± 2	25 ± 1	...	...
1015+161	19 950	7.92	15.61	0.58	1.73	7.78	196 ± 9	166 ± 8	146 ± 7	128 ± 7
1017+125	21 390	7.88	15.67	0.56	1.53	7.60	73 ± 3	48 ± 2	27 ± 3	18 ± 6
1018+410	22 390	8.04	16.37	0.65	2.37	7.66	85 ± 4	74 ± 3	...	...
1020–207	19 920	7.93	15.04	0.58	1.74	7.79	130 ± 6	83 ± 4	...	...
1034+492	20 650	8.17	15.43	0.73	3.05	7.94	100 ± 5	58 ± 3	48 ± 3	28 ± 5
1038+633	24 450	8.38	15.15	0.86	4.31	7.90	108 ± 5	67 ± 3	57 ± 3	17 ± 4

WD	$T_{\rm eff}$ (K)	$\log g$ [$\log(\mathrm{cm\,s^{-2}})$]	V (mag)	$M_{\rm wd}$ ($M_\odot$)	$M_{\rm ms}$ ($M_\odot$)	$\log(t_{\rm cool})$ [$\log(\mathrm{yr})$]	$F_{3.6\,\mu\mathrm{m}}$ (μJy)	$F_{4.5\,\mu\mathrm{m}}$ (μJy)	$F_{5.7\,\mu\mathrm{m}}$ (μJy)	$F_{7.9\,\mu\mathrm{m}}$ (μJy)
1049+103	20 550	7.91	15.81	0.58	1.67	7.71	3743 ± 187	2579 ± 129	...	...
1049–158	20 040	8.28	14.36	0.79	3.65	8.08	256 ± 12	155 ± 7	...	...
1052+273	23 100	8.37	14.12	0.86	4.23	7.98	304 ± 15	193 ± 9	129 ± 7	59 ± 7
1058–129	24 310	8.71	14.91	1.06	6.10	8.20	128 ± 6	81 ± 4	41 ± 6	29 ± 8
1102+748	19 710	8.36	15.05	0.84	4.13	8.18	136 ± 6	89 ± 4	...	...
1104+602	17 920	8.02	13.74	0.63	2.17	8.04	463 ± 23	293 ± 14	...	...
1115+166	22 090	8.12	15.05	0.70	2.80	7.77	133 ± 6	85 ± 4	69 ± 4	43 ± 6
1122–324	21 670	7.86	15.82	0.55	1.44	7.55	62 ± 3	40 ± 2	...	...
1129+155	17 740	8.03	14.09	0.64	2.22	8.06	376 ± 18	234 ± 11	159 ± 8	78 ± 7
1133+293	23 030	7.84	14.88	0.55	1.41	7.39	146 ± 7	90 ± 4	63 ± 6	43 ± 8
1134+300	21 280	8.55	12.45	0.96	5.23	8.26	1382 ± 69	889 ± 44	...	...
1136+139	23 920	7.83	...	0.54	1.37	7.28	22 ± 2	15 ± 1	...	...
1201–001	19 770	8.26	15.16	0.78	3.55	8.08	124 ± 6	80 ± 4	48 ± 3	17 ± 3
1204–322	21 260	8.00	15.62	0.62	2.12	7.72	80 ± 4	52 ± 2	...	...
1229–013	19 430	7.47	14.46	0.38	...	7.54	239 ± 12	152 ± 7	90 ± 5	64 ± 7
1230–308	22 760	8.28	15.73	0.80	3.71	7.90	69 ± 3	45 ± 2	...	...
1233–164	24 890	8.21	15.10	0.76	3.33	7.66	114 ± 5	72 ± 3	...	...
1243+015	21 640	7.82	16.46	0.53	1.27	7.52	33 ± 1	23 ± 1	...	...
1249+182	19 910	7.73	15.24	0.49	0.85	7.65	95 ± 4	60 ± 3	...	...
1257+048	21 760	7.95	14.94	0.60	1.89	7.62	150 ± 7	97 ± 4	...	...
1310–305	20 350	7.82	14.48	0.53	1.25	7.66	223 ± 11	143 ± 7	...	...
1323–514	19 360	7.76	14.39	0.50	0.98	7.73	275 ± 13	175 ± 8	...	...
1325+279	21 270	8.04	15.80	0.65	2.35	7.76	63 ± 7	42 ± 4	...	...
1325–089	17 020	7.81	...	0.52	1.12	8.00	165 ± 8	107 ± 5	...	...
1330+473	22 460	7.95	15.23	0.60	1.91	7.55	106 ± 5	70 ± 3	...	...
1334–160	18 650	8.32	...	0.82	3.86	8.20	116 ± 6	98 ± 5	...	...
1335+369	20 510	7.78	...	0.51	1.08	7.62	2056 ± 102	1326 ± 66	...	...
1337+705	20 460	7.90	12.60	0.57	1.62	7.71	...	709 ± 35	...	254 ± 13
1338+081	24 440	7.65	16.44	0.47	0.66	7.20	30 ± 1	19 ± 1	...	...
1353+409	23 530	7.59	15.49	0.44	...	7.26	76 ± 3	50 ± 2	32 ± 4	26 ± 5
1408+323	18 150	7.95	13.97	0.59	1.81	7.97	...	251 ± 12	...	92 ± 7
1433+538	22 410	7.80	16.14	0.53	1.21	7.43	906 ± 45	632 ± 31	...	...
1449+168	22 350	7.79	15.39	0.52	1.15	7.42	91 ± 4	58 ± 2	...	...
1451+006	25 480	7.89	15.27	0.58	1.69	7.16	98 ± 5	63 ± 3	...	...
1452–042	23 530	8.19	16.29	0.74	3.21	7.74	51 ± 2	36 ± 2	...	...
1457–086	21 450	7.97	15.76	0.61	1.99	7.68	113 ± 5	73 ± 3	48 ± 3	...
1459+347	21 520	8.48	15.79	0.92	4.84	8.18	65 ± 3	41 ± 2	...	...
1507+220	19 870	7.75	14.95	0.49	0.91	7.66	150 ± 7	96 ± 4	...	...
1524–749	23 090	7.74	15.99	0.50	0.99	7.32	64 ± 3	39 ± 2	...	...
1525+257	22 290	8.28	15.73	0.80	3.70	7.93	69 ± 3	44 ± 2	...	...
1527+090	21 200	7.85	14.30	0.55	1.39	7.59	259 ± 13	164 ± 8	...	...
1531–022	18 620	8.41	13.97	0.87	4.41	8.30	...	243 ± 12	...	103 ± 8
1533–057	20 000	8.50	15.38	0.93	4.94	8.29	94 ± 4	57 ± 2	...	...
1535+293	24 470	7.92	...	0.59	1.81	7.30	50 ± 2	30 ± 1	...	...
1547+057	24 360	8.36	15.94	0.85	4.16	7.88	56 ± 2	36 ± 1	...	...
1548+149	21 450	7.86	15.16	0.55	1.45	7.57	122 ± 6	77 ± 3	...	...
1614+136	22 020	7.21	15.23	0.32	...	7.23	113 ± 5	67 ± 3	54 ± 5	15 ± 5
1620–391	24 680	7.93	11.00	0.60	1.85	7.29	4988 ± 249	3113 ± 155	1936 ± 96	1073 ± 53
1633+676	23 660	7.97	16.25	0.62	2.04	7.45	34 ± 1	21 ± 1	...	...
1647+375	21 980	7.89	14.91	0.57	1.61	7.55	137 ± 6	86 ± 4	...	...
1713+332	22 120	7.43	14.39	0.38	...	7.32	...	184 ± 9	...	57 ± 6
1755+194	24 440	7.80	15.99	0.53	1.28	7.21	54 ± 3	33 ± 1	...	...
1914–598	19 760	7.84	...	0.54	1.31	7.74	288 ± 14	196 ± 10	...	...
1929+012	20 890	7.91	14.20	0.58	1.68	7.68	837 ± 41	781 ± 39	...	...
1943+163	19 760	7.79	13.95	0.51	1.11	7.71	...	230 ± 11	...	100 ± 7
1953–715	19 270	7.87	15.06	0.55	1.47	7.81	132 ± 6	84 ± 4	...	...
2021–128	20 750	7.82	15.20	0.53	1.26	7.62	112 ± 5	74 ± 3	...	...
2032+188	18 200	7.36	15.32	0.34	...	7.58	125 ± 6	80 ± 4	...	...
2039–202	19 740	7.79	12.33	0.51	1.08	7.70	...	1035 ± 51	...	371 ± 20
2046–220	23 410	7.83	15.37	0.54	1.36	7.33	88 ± 4	55 ± 2	...	...
2058+181	17 350	7.75	15.20	0.49	0.88	7.94	149 ± 7	97 ± 5	...	...
2134+218	18 000	7.86	14.48	0.55	1.39	7.93	...	158 ± 8	...	61 ± 6
2149+021	17 930	7.86	12.76	0.54	1.38	7.94	...	776 ± 38	...	272 ± 15
2152–045	19 840	7.38	15.69	0.35	...	7.44	83 ± 4	52 ± 2	...	...
2200–136	24 730	7.61	15.33	0.45	0.53	7.19	106 ± 5	66 ± 3	...	...

WD	$T_{\rm eff}$ (K)	$\log g$ [$\log(\mathrm{cm\,s^{-2}})$]	V (mag)	$M_{\rm wd}$ ($M_\odot$)	$M_{\rm ms}$ ($M_\odot$)	$\log(t_{\rm cool})$ [$\log(\mathrm{yr})$]	$F_{3.6\,\mu\mathrm{m}}$ (μJy)	$F_{4.5\,\mu\mathrm{m}}$ (μJy)	$F_{5.7\,\mu\mathrm{m}}$ (μJy)	$F_{7.9\,\mu\mathrm{m}}$ (μJy)
2204+071	24 450	7.95	15.78	0.61	1.95	7.34	68 ± 3	41 ± 2	...	...
2210+233	23 230	8.24	15.84	0.77	3.48	7.82	59 ± 3	34 ± 1	...	...
2220+133	22 580	8.30	15.61	0.81	3.82	7.93	75 ± 3	45 ± 2	...	...
2220+217.1	18 740	8.24	15.22	0.77	3.43	8.13	79 ± 4	45 ± 2	...	...
2229+235	19 300	7.90	16.01	0.57	1.60	7.83	59 ± 3	38 ± 2	23 ± 2	...
2231–267	21 590	7.99	14.97	0.62	2.09	7.68	162 ± 8	108 ± 5	...	...
2238–045	17 540	8.18	16.90	0.73	3.04	8.17	22 ± 1	13 ± 0	...	...
2244+210	24 110	7.89	16.45	0.57	1.66	7.31	35 ± 1	21 ± 1	...	...
2257+162	24 580	7.49	15.97	0.41	...	7.24	417 ± 20	287 ± 14	195 ± 10	128 ± 8
2306+124	20 360	7.99	15.08	0.62	2.08	7.80	124 ± 6	76 ± 3	...	...
2322–181	21 680	7.90	15.28	0.57	1.65	7.59	99 ± 5	61 ± 3	...	...
2328+107	21 000	7.78	15.76	0.51	1.08	7.56	115 ± 5	77 ± 3	...	...
2359–324	22 480	7.74	16.26	0.50	0.97	7.38	43 ± 2	27 ± 1	...	...